Available online at www.sciencedirect.com
SCIENCE DIRECT®
International Journal of Mass Spectrometry 231 (2004) 37–45
International Journal of Mass Spectrometry
www.elsevier.com/locate/ijms

Design and performance of a new FT-ICR cell operating at a temperature range of 77–438 K

Xinghua Guo [a], Marc Duursma [a], Ahmed Al-Khalili [a], Liam A. McDonnell [a], Ron M.A. Heeren [a,b,*]

[a] *FOM Institute for Atomic and Molecular Physics, Kruislaan 407, Amsterdam SJ 1098, The Netherlands*
[b] *Department of Biomolecular Mass Spectrometry, Bijvoet Center for Biomolecular Research, Utrecht University, Sorbonnelaan 16, Utrecht CA 3584, The Netherlands*

Received 27 June 2003; accepted 26 August 2003

Abstract

A new ion cell for Fourier transform ion cyclotron resonance mass spectrometry (FT-ICR-MS), which can be operated within the temperature range 77–438 K, has been designed and constructed. It has an elongated open-ended cylindrical configuration with capacitively coupled trapping electrodes. Fast and accurate thermal control of the cell is realized by embedding a heating element and a cooling pipe into the ceramic jacket holding the cell electrode plates. To determine the geometry factor, β, of the cell a novel empirical methodology has been developed that is applicable to any ICR cell. This was achieved by comparing breakdown diagrams of protonated leucine enkephalin obtained using the new cell with those obtained using a well characterized cell.

Energy-resolved collision-activated dissociation (CAD) of protonated leucine enkephalin, performed using the new cell, was applied to probe the internal energy content of ions at different ICR cell temperatures. These experiments demonstrate that the trapped ion population reaches the preset temperature of the cell through thermal equilibration with the cell walls by blackbody infrared radiation. This has permitted FT-ICR-MS studies (dissociation or ion–molecule reactions, etc.) to be performed at a wide temperature range, including low temperatures.

Keywords: Temperature-controlled ICR cell; FT-ICR-MS; Low temperature mass spectrometry; Geometry factor

1. Introduction

Fourier transform ion cyclotron resonance mass spectrometry (FT-ICR-MS) [1] has proven to be a powerful tool for both fundamental [2] and (bio-)analytical [3] chemical studies. Its ultra-high mass resolution, ion trapping, ion–molecule reactions and MS^n capabilities combined with modern ionization techniques, such as electrospray ionization (ESI) [4] and matrix-assisted laser desorption ionization (MALDI) [5], have made it one of the most structurally informative techniques available. FT-ICR-MS has been exploited to provide valuable information in many different fields, ranging from organic/organometallic ions [6] to biological complexes [7]. Its main impact, for example in biomolecular analysis [8], results from its ability to trap ions for tandem mass spectrometric investigation with high resolution and mass accuracy.

The vast majority of FT-ICR-MS studies are performed at room temperature. Nevertheless, experiments performed at elevated temperatures have been shown to provide additional analytically useful information (with respect to experiments performed at room temperature) as well as fundamental insights into the chemistry of large molecular ions. Examples include blackbody infrared radiative dissociation (BIRD) [9], ion–molecule reactions [10] and electron capture dissociation [11] at elevated temperatures. BIRD has been used to determine activation energies for the thermal dissociation of biological macromolecules [12] and non-covalent complexes [13,14] while ion–molecule reactions can provide information about the structures of the individual molecules and clusters [10].

These studies are possible due to the long ion storage time in an ICR cell, which allows the ions to reach a thermal equilibrium with the cell electrodes. Normally, the cell is heated indirectly, in that the cell is heated with blackbody

* Corresponding author. Tel.: +31-20-6081234; fax: +31-20-6684106.
E-mail address: heeren@amolf.nl (R.M.A. Heeren).

1387-3806/$ – see front matter © 2003 Elsevier B.V. All rights reserved.
doi:10.1016/j.ijms.2003.08.016

infrared radiation from a directly heated vacuum chamber. Because most systems have not been designed with a view to controlling the temperature of the cell, the heat transfer characteristics have not been considered. As a result, the temperature of the cell must be calibrated against the temperature of the external vacuum chamber. Furthermore, the temperature distribution within such non-optimized cells is not uniform [14]. This makes it difficult to accurately define the temperature of the ion population, which is essential in order to extract the activation energy for dissociation from an Arrhenius plot. Finally, depending on the desired temperature, indirect heating can require a long heating time (10 h to 2 days) to allow the cell to reach a relatively stable temperature.

In our previous study, a cylindrical ICR cell with a heating element was described that can be used to increase the temperature of the ion population up to 450 K [15]. One important feature of this cell is that it produces a thermally controlled and spatially uniform hot environment. Consequently, the ion internal energies could be controlled and described by a single temperature. In a recent study, BIRD was performed using heated filaments (resistant wire) adjacent to the cell excitation/detection plates [16]. Although the temperature of the filaments was estimated to be as high as 2000 K, this experimental setup would result in an inhomogeneous temperature distribution within the cell and the temperature of the ion population poorly defined.

In contrast to these studies at high temperatures, to our best knowledge there have been few reports about studying ion structures, conformations and reactivities at temperatures lower than room temperature in FT-ICR-MS. BIRD of hydrated metal complexes at low temperature has been studied using a cooled-cell in FTICR using indirect cooling surrounding cell region and at a recent conference Lee et al. [17] discussed the design and construction of a cryo-cooled cell. Note ion–molecule reaction rates [18] and the formation of cluster ions [19] have also been studied at low temperatures using a drift tube mass spectrometer. The new ICR cell reported here has been designed with a view to investigate the temperature dependence (both below and above room temperature) of the conformations of gas-phase biological macromolecular ions. A basic tenet of modern biology is that the conformations of biomolecules play a fundamental role in their bioactivities, specifically through non-covalent interactions. Mass spectrometry has been widely applied to investigate the conformations and non-covalent interactions between large biomolecules [20]. A key question in the latter studies is whether the conformations of gas-phase multiply charged biomolecules are related to those in solution. Although some experimental evidence has demonstrated that gas-phase biomolecular ions produced from ESI sources reflect those in the solution phase [21], later studies [22] combining ion mobility and mass spectrometry indicate that multiply protonated proteins undergo rapid conformational changes (folding/unfolding) during the first milliseconds to seconds after ionization/volatilization. This experimental evidence [22] indicates that the gas-phase conformations are sensitive to the charge state and the internal energy of the ions, irrespective of whether the internal energy is supplied through blackbody infrared radiation or collisional heating. A spatially uniform temperature-controlled cell, for temperatures above and below room temperature, allows ions to be prepared with a well-defined (by a single temperature) Boltzmann distribution of internal energies. Consequently, the temperature dependence of macromolecular ion conformations, ion–molecule reactions (normally used to investigate macromolecular ion conformations), and macromolecular ion dissociation can be investigated. In this paper a new temperature-controlled FT-ICR ion cell with both a direct heating element and a cooling system is described.

2. Details of the new ICR cell

2.1. Construction of the new ICR cell

In FT-ICR mass spectrometry, many different types of ICR cells have been developed [23]. These include the early cubic cell [24], analogue cells with hyperboloidal electrodes [25], close-ended cylindrical cells [26], the “infinity” cell [27], and open-ended cylindrical cells [28,29]. Most ICR cell geometries utilize trapping electrodes situated on both sides of the cell to constrain the axial motion of the ions within the cell. These electrodes are typically either plates (with a small hole to allow ions to enter the cell) or offset extensions of the cell, creating closed and open cells, respectively. Ion cells with a closed geometry have only a restricted access to the cell interior, which limits external ion injection, reduces sensitivity [30], and can suffer from mass-dependent ion loss and mass discrimination during excitation events [31]. Contrarily cells with an open-ended geometry [28,29,32] overcome most of the above-mentioned restrictions.

A schematic diagram of the new FT-ICR cell is shown in Fig. 1a. As can be seen it has a central excite/detect segment flanked by two trapping segments and is of cylindrical geometry (a cylindrical open cell). All of the copper (oxygen free) electrodes have an inner diameter of 60 mm and the lengths of the excitation/detection and trapping segments are 100 and 50 mm, respectively. The elongated configuration reduces space-charge effects, consequently the mass spectra are less prone to the frequency shifts due to population variations in the cell [32]. Note the automatic gain control recently described will decrease this problem still further (though it reduces the duty cycle) [33].

The excitation and detection electric circuits are shown in Fig. 1b. Each trapping segment resembles the excitation/detection segment in that they are divided into four identical sectors. These trapping sectors are serially connected to each other through four resistors (150 kΩ) and the dc trapping voltage is applied to this reconstructed cylinder electrode through another 150 kΩ resistor. In addition, each trapping sector adjacent to an excitation sector (of the

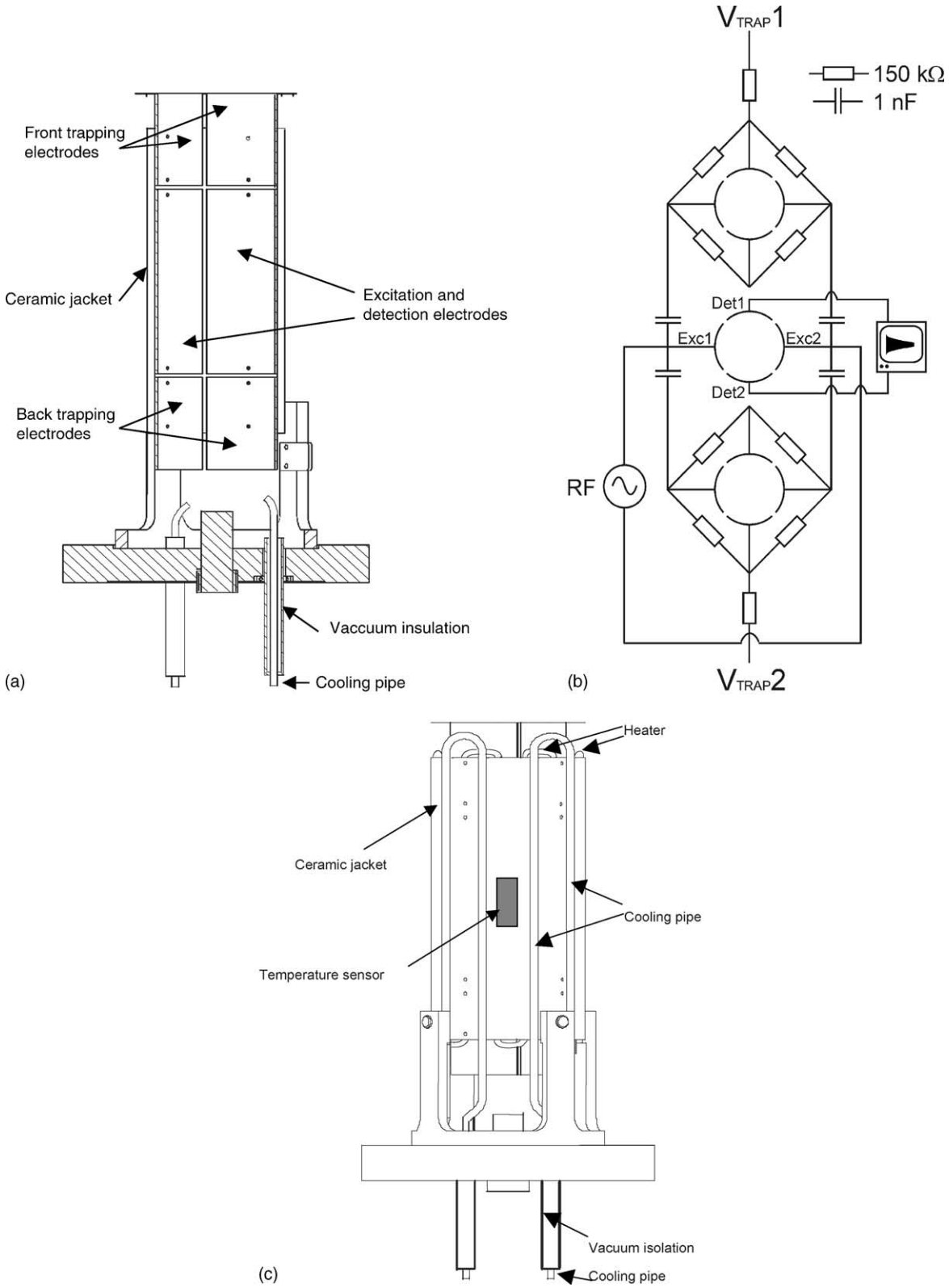

Fig. 1. Schematics of the new ICR cell: (a) cross section, (b) excitation and detection circuits, and (c) side view.

excitation/detection segment) is capacitively coupled to the excitation electrodes by a 1 nF capacitor. As a result, during excitation the ions experience a more homogeneous RF excitation field [28,32,34].

The electrodes are mounted in a ceramic cylinder (99.7% Al_2O_3 (Alsint), Haldenwanger, Berlin, Germany) with an internal diameter of 61 mm and an outer diameter of 80 mm. The interior of the ceramic wall contains 12 coaxial holes of 3 mm diameter. Within these channels resides a shielded heater element, see Fig. 1c. This heater element (type T538809, Rossel, Alphen a/d Rijn, The Netherlands) consists of an outer rigid copper cylinder, a co-axial mineral isolation material (MgO) and a Cr/Ni central heater wire of 0.5 mm diameter with a specific resistance of 2 Ω/m. This heater element was chosen as it can be electrically shielded from the ICR cell electrodes, thus preventing the introduction of electronic noise from the heater current and the heater current can be kept sufficiently low so as to have only a minimal effect on the magnetic field homogeneity. The total resistance of the heater elements was measured to be about 4.5 Ω at room temperature. Tests have shown that it could provide up to 45 W output of heating power.

In addition to the heating wire, the new ICR cell also contains a cooling system. This cooling system consists of a copper pipe partially enclosed in the ceramic jacket of the cell, through which a liquid or gas is flowed (see Fig. 1c). The inner and outer diameters of the cooling pipe are 3 and 5 mm, respectively. This pipe is wrapped around the outer ceramic wall in 16 parallel channels. For both heating and cooling elements, the ceramic acts as a heat sink that ensures a spatially uniform temperature distribution at the centre of the ICR cell. Using this combination of a heater, a cooling device and a heat sink the temperature of the cell can be varied between 77 and 500 K while maintaining a uniform temperature distribution. Up to date, using this cell protein spectra have been recorded throughout the temperature range 77–438 K.

The temperature is measured with a Pt100 temperature sensor that is embedded into the ceramic wall. A temperature regulator (type: 2416, Eurotherm BV, Alphen a/d Rijn, The Netherlands) was used to measure the temperature of the cell. The output was recorded with a PC computer using LabVIEW [35]. Note that because of intermittent noise pick-up from the Eurotherm regulator during ion detection, it was disconnected from the Pt100 thermal sensor during the MS acquisition and only switched on between the MS scans.

The ceramic jacket and the ICR cell electrodes are mounted on a standard CF flange with the cooling pipe situated away from the detection feed-through. In order to avoid water condensation and ice formation in the preamplifier (situated immediately behind the flange), the cooling pipe is vacuum-isolated. A co-axially mounted stainless tube (10 mm inner diameter) surrounds both ends of the cooling pipe while it is passing through the flange and the preamplifier. As a result, the cooling gases/liquids can be easily passed through the pipe without affecting the performance of the preamplifier.

2.2. Thermal behavior of the new ICR cell

The thermal behavior of the new temperature-controlled cell was evaluated. To test the performance the heater element was powered and the temperature of the cell was recorded as a function of time. Curve (a) in Fig. 2 shows an example of a typical cell–temperature curve of the cell using 28 W heating power. As can be seen, there is sharp initial rise in temperature that gradually plateaus to give a steady temperature. After approximately 450 min, the heater power was switched off and the cell began to passively cool through the emission of blackbody infrared radiation. The final temperature of the cell and time taken to reach this final temperature are dependent on the heater power, for instance approximately 180 min at 42 W are needed to reach a steady temperature of 500 K.

Curve (b) in Fig. 2 shows that it was not possible to reach any temperatures above 375 K through indirect heating. To obtain this curve the bake-out system was used to heat the outside surface of the vacuum housing to a final temperature of 448 K. However, at thermal equilibrium the temperature difference between the ICR cell and the vacuum housing was still 77 K.

In order to regulate the cell temperature during direct heating, the working curve of the final cell temperature (T) under thermal equilibrium versus the heating power (W) was measured and is shown in Fig. 3. Using this curve the cell temperature can be arbitrarily set within a wide range above room temperature by simply changing the heating power. The temperature of the ICR cell can then be maintained at a constant value for a relatively long period of time with a maximum ±3 K variation in 30 min for temperatures up to 500 K (see Fig. 3). In contrast, for indirect heating such high temperatures are problematic because the hot vacuum housing (which must be maintained for a long time to obtain a steady temperature) causes the magnet cryogen to be lost at a faster rate and the high temperatures can adversely affect the detection preamplifier (normally mounted on the vacuum housing close to the cell to minimize noise). Using a directly heated cell, the temperature rise of the surrounding vacuum housing is minimized.

In a routine experiment, the ICR cell is heated close to the desired temperature with a higher power applied to the heater. Subsequently the heating power is switched to the value corresponding to the desired temperature according to Fig. 3. For example, to set up the temperature of the cell to 393 K, as shown in curve (c) of Fig. 2, the cell was first heated up with 42 W (for 1 h) to 390 K then switched to 14 W. The cell temperature was then kept at 393 ± 3 K for more than 2 h.

The thermal behavior of the new temperature-controlled ICR cell at low temperatures was studied using liquid nitrogen as a cooling agent. A steady flow of liquid nitrogen was

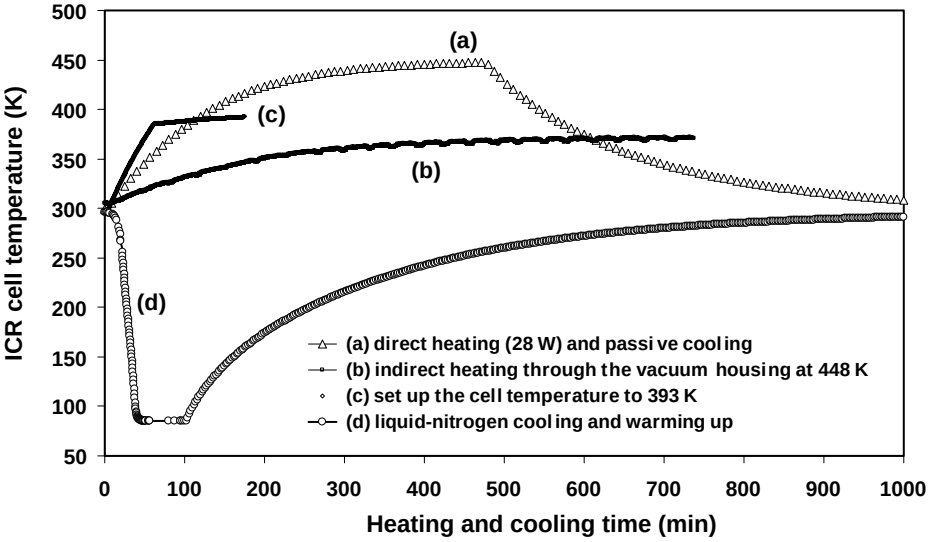

Fig. 2. The temperatures of the new temperature-controlled cell versus time: (a) directly heated with 28 W for 450 min and then allowed to passively cool to room temperature, (b) indirectly heated up through the vacuum chamber; note that the vacuum chamber reached 448 K within 20 min, however, the cell only reached a constant temperature, 371 K, after 700 min. The final temperature difference between the vacuum housing and the cell is 77 K under a thermal equilibrium, (c) the setup of the cell temperature during experiments: the cell was first heated with 42 W (for 1 h) to 390 K then switched to 14 W. The final cell temperature was then kept at 390 ± 3 K for more than 2 h, (d) directly cooled down with liquid nitrogen to 77 K and then warmed up to room temperature.

introduced through the cooling line of the new cell while the temperature of the cell was monitored. Curve (d) in Fig. 2 shows the resulting temperature curve for a liquid N_2 flow rate of 3 l/h and demonstrates that the entire cell could be cooled down to 77 K (the boiling point of liquid nitrogen) within 40 min. After approximately 100 min the liquid nitrogen flow was stopped and the cell returned to room temperature. During the MS experiments at low temperatures, a low flow rate of liquid nitrogen, which is dependent on the desired temperatures, was applied to keep the ICR cell at a constant low temperature. Similar to the procedure outlined above for high temperatures, this was done after the cell was first cooled down close to the desired temperature. Using this technique the cell could be cooled rapidly and the final temperature kept constant with an accuracy of ± 3 K for >30 min.

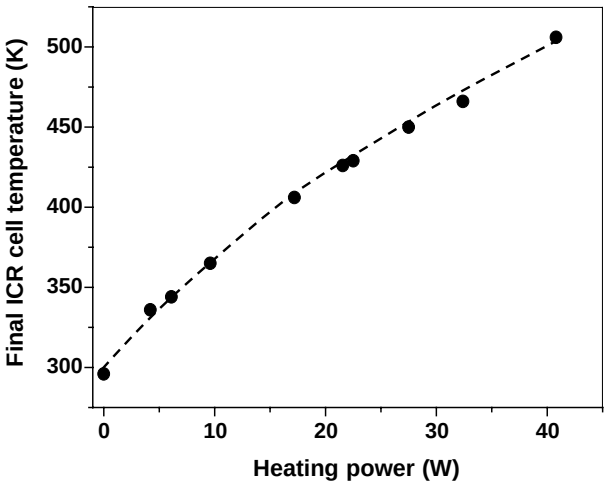

Fig. 3. The dependence of the final temperature of the temperature-controlled cell on the heating power of the heater element.

3. Experimental

The new ICR cell was mounted onto a modified Bruker APEX 7.0e FT-ICR mass spectrometer equipped with an external ESI source and an arbitrary waveform generator (AWG) [36]. Fifty micromoles of leucine enkephalin (YGGFL) (Sigma Chemical Co., St. Louis, MO, USA) in a mixture of methanol:water:AcOH, 69:29:2 (vol.%) was either nano- or micro-electrosprayed. The protonated molecules ($[M+H]^+$, m/z 556) were trapped in the ICR cell and isolated by applying a RF excitation chirp generated with the AWG that ejected all unwanted ions [36]. After the pump-probe experiments, in which a thermalization delay is used to pump the ion population to the cell temperature (via blackbody infrared radiation) and collision-activated dissociation used to probe the internal energies of the ion population, the ions were detected with a 1.02 ms, ~200 V chirp excitation pulse followed by a 0.209 s broadband acquisition with a bandwidth of 312.5 kHz.

This pump-probe methodology has been described extensively in our recent studies [15,37–39] and was used here to investigate the initial internal energy of the ion population for different cell temperatures. Under equilibrium conditions the internal energy of the trapped ion population is assumed to have a Maxwell–Boltzmann distribution, characterized by a single temperature. The initial internal energy distribution of the ion population is expressed by a breakdown diagram [40], which is the curve of the ion survival yield (the ratio

between precursor ion intensity and the sum of the intensities of precursor and fragment ions) versus the collision energy during CAD in collisional (or internal) energy-resolved dissociation studies.

Details on how to construct breakdown diagrams at different temperatures using CAD have been published previously [15,39]. Briefly, after the ICR cell was thermalized at a chosen temperature, the ions generated in the external ESI source were transferred into and trapped in the ICR cell. A 3 s argon gas pulse was then used to moderate the kinetic energy of the ions (peak pressure 5×10^{-6} mbar). After a background pressure of less than 1×10^{-8} mbar was reached a delay of up to 60 s was used to thermally equilibrate the ions with the hot or cold cell walls. This delay was found to be sufficient to thermalize the ion cloud, in agreement with previous work [41]. The ions were then probed by a series of on-resonance CAD experiments (with argon as collision gas, 3 s, peak pressure at 5×10^{-6} mbar) with different collisional activation energies to induce dissociation. Finally the ion survival yield of the precursor ions is plotted versus the laboratory-frame kinetic energy.

At cell temperatures of about 87 K argon (with the boiling point of 87 K) started to condensate on the cold cell. Consequently the pressure of the collision gas argon decreased dramatically. This resulted in a lower degree of fragmentation. Therefore, for collision induced dissociation and ion–molecule reactions at low temperatures, it is necessary to use a neutral gas with a boiling point lower than the temperature of the ICR cell. Below 87 K, helium (with a boiling point of 4 K) will become the only applicable collision gas in FT-ICR-MS. Considering the lower center-of-mass collision energy when using helium and the rapid increase in infrared cooling with decreasing temperature (of the cell), a limit is expected where collision-activated dissociation is no longer effective. Such a limit has been observed in low energy SORI-CID experiments performed at 178 K using this cell [38]. Though the possibility of performing FTMS at 4.2 K will lead to significant signal/noise, sensitivity and dynamic range gains [42], in light of the observations CAD experiments at this temperature will be difficult.

4. Results and discussion

4.1. Determination of the geometry factor of the new ICR cell

In order to perform collisional activation, ion detection and ion ejection in FT-ICR-MS, ions need to be excited to "large" cyclotron orbits with high kinetic energies. The maximum kinetic energy of ions can be calculated with the equation: $E_{\mathrm{kin,lab}} = \beta^2 q^2 V_{\mathrm{p-p}}^2 t_{\mathrm{exc}}^2/(8md^2)$, in which β is the geometry factor of the cell, $V_{\mathrm{p-p}}$ and t_{exc} are the peak-to-peak amplitude and the duration of the RF excitation, q and m are the number of charge and the mass of the ions, respectively, and d is the diameter of the excitation/detection electrodes. All of these parameters can be measured or were known for the newly constructed temperature-controlled ion cell except the geometry factor β. The geometry factor of an ICR cell is a parameter influencing the kinetic energy of ions by affecting the power absorption during ion excitation for detection/activation [43]. It depends exclusively on the geometry of an ICR cell. In the literature there are only a few types of ICR cells available with known geometry factors, these were determined either theoretically [44,45] or experimentally [46].

As mentioned in the introduction, the geometry factor β is a characteristic parameter of an ICR cell and is dependent on its geometrical dimensions (length and width). It is usually proportional to the aspect ratio α of an ICR cell [32] with a constant of proportionality, A (that is dependent on the cell), less than 1 ($\beta = A \times \alpha$, $A < 1$) [45,46]. In the case of an elongated open-ended cylindrical cell with the length of the trap electrodes similar to that of the excitation electrodes, the aspect ratio α is defined [32] by the distance between the trap potential maxima divided by the cell width. Using the theoretical distance between the trap potential maxima obtained using SIMION [47] calculations that included all of the electrodes near the cell and vacuum housing, the aspect ratio α of the new open cell was calculated to be 2.46 (147.6/60).

A new experimental protocol was used to determine the geometry factor β of the new temperature-controlled ICR cell. By comparing the room temperature on-resonance CAD breakdown diagram of protonated leucine enkephalin obtained with a Bruker InfinityCell (assuming a known geometry factor of 0.897 [44]) with that acquired with the new temperature-controlled open cell under identical experimental conditions, the geometry factor was determined. Typical room temperature breakdown diagrams of protonated leucine enkephalin obtained using the Bruker InfinityCell and the new temperature-controlled cell are shown by the curves (a) and (b) in Fig. 4 respectively. The 'kinetic energies' of the curve (b) in Fig. 4 were calculated by as-

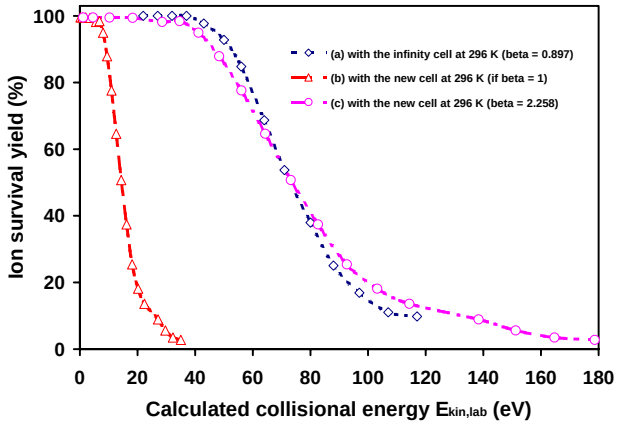

Fig. 4. A comparison of the breakdown diagrams of protonated leucine enkephalin obtained at room temperature 296 K: (a) using the Bruker InfinityCell with a known geometry factor [44] β of 0.897; (b) using the new temperature-controlled cell in this work by assuming $\beta = 1$; and (c) using the new temperature-controlled cell in this work with $\beta = 2.26$.

suming the geometry factor $\beta = 1$. This figure illustrates both the method of and the need for the determination of the geometry factor.

One of the basic assumptions [39] in this study is that an ion survival yield of 50% corresponds to the mode average of the total (final) internal energy distribution $E^{\text{int}}_{\text{total mode}}$ of the activated ion population. For thermal distributions at mild temperatures, the median (50%) and mode averages are similar and quite insensitive to small changes of the distribution. Here blackbody infrared radiation (by changing the cell temperature) is used to increase the temperature of the ion population, and collisional activation dissociation is used to probe their internal energy. At a given temperature T, the mode of the total (final) internal energy distribution $E^{\text{int}}_{\text{total mode}}$ of the activated ion population consists of two contributions: $E^{\text{int}}_{\text{total mode}} = E^{\text{int}}_{\text{ini,mode}}(T) + E^{\text{int}}_{\text{dep}}(T)$, where $E^{\text{int}}_{\text{ini,mode}}$ is the initial internal energy distribution acquired from blackbody infrared radiation (characterized by the temperature T) and $E^{\text{int}}_{\text{dep}}$ is the deposited internal energy distribution acquired during collisional activation.

The experiments to determine the geometry factor were performed at room temperature, therefore, the initial internal energy $E^{\text{int}}_{\text{ini,mode}}(T)$ was fixed. To reach the same 50% ion survival yield, the contribution of collisional activation, $E^{\text{int}}_{\text{dep}}(T)$, and the kinetic energy, $E_{\text{kin, lab}}$, must be constant, irrespective of how the ions are collisionally activated in the different ICR cells.

In Fig. 4 by imposing the condition that the laboratory-frame kinetic energy corresponding to a 50% ion survival yield of the breakdown diagram obtained using the new temperature-controlled cell is identical to that obtained using the Bruker InfinityCell, the geometry factor β of the new temperature-controlled ICR cell was determined to be 2.26 (using the equation $E_{\text{kin,lab}} = \beta^2 q^2 V^2_{p-p} t^2_{\text{exc}}/8md^2$). As a result, the original $\beta = 1$ curve (b) is shifted to curve (c). The observation that curves (a) and (c) deviate from each other at positions other than the 50% point, most likely reflects different broadening effects of the internal energy distribution under the different experimental conditions [39].

The geometry factor β of 2.26 determined using this empirical approach is reasonable ($A = 0.92$) when compared to the reported geometry factors for similar ICR cells [45,46]. This value was used to calculate the laboratory-frame kinetic energies of the CAD experiments reported here and in other studies [37–39]. This empirical determination of the relative geometry factor (relative to the geometry factor of the infinity cell) introduces a universal and simple methodology that can be applied to any custom-made ICR cell.

4.2. Internal energy changes of ion populations thermalized in the temperature-controlled cell: breakdown diagrams at high, room, and low temperatures

Firstly, the performance of the temperature-controlled ICR cell (and thermalized ion populations) was investigated at temperatures ranging from 77 to 438 K. Studies were performed using both small peptides and larger proteins such as cytochrome *c* and myoglobin. The mass spectra at high and low temperatures are similar to those obtained at room temperatures. This indicates that in the time scale of the experiments no BIRD occurred at the high temperatures. For the proteins investigated a similar charge state distribution was observed at all temperatures provided the electrospray and trapping conditions were identical.

Finally, the relation between the cell temperature and internal energy change of the equilibrated ion population was evaluated. Protonated leucine enkephalin ions generated in the external ESI source were transferred to and trapped in the new temperature-controlled cell at a given cell temperature. As described earlier breakdown diagrams were constructed to determine the energy dependence of the dissociation process using on-resonance CAD. At all of the temperatures studied here the molecular ions of leucine enkephalin dissociated into two main fragments, namely m/z 425 (b_4 ions) and m/z 397 (a_4 ions). This indicates that the ions had accumulated a similar amount of internal energy prior to fragmentation. A comparison of the breakdown diagrams of protonated leucine enkephalin obtained at cell temperatures of 393, 296, and 173 K with on-resonance CAD is shown in Fig. 5. The corresponding kinetic energies for a 50% ion survival yield are 62.8, 80.5, and 101 eV, respectively. With respect to the breakdown diagram obtained at room temperature, curve (b), it is clear that the breakdown diagram obtained at 393 K, curve (a), was shifted to lower kinetic energies. In contrast, the breakdown diagram obtained at 173 K, curve (c), was shifted to higher kinetic energies. Assuming the ions reach the preset temperatures of the ICR cell before collisional activation, the most probable (mode average) internal energies of the ion populations before collisional activation at 393, 296, and 173 K are 1.54, 0.90, and 0.31 eV, respectively, calculated using the active oscillator model of Drahos and Vekey [48]. For all but the very highest temperatures, these energies are very similar to the median average energies of the distribution [40]. Accordingly, these energies were used to characterize the initial internal energy of the ions in the analysis of the 50% ion survival yield points of the breakdown diagrams [39]. With respect to room temperature, the most probable initial internal energies of the ion populations changed by +0.64 (at 393 K) and −0.59 eV (at 173 K). The corresponding kinetic energies at the 50% ion survival yield points of the breakdown diagrams were shifted by −17.7 and 20.5 eV, respectively. It is readily apparent that as the temperature decreased higher collision energies (and thus more deposited internal energy) were required. These higher kinetic energies are needed to reach the internal energy required to achieve 50% fragmentation, and compensated for the lower initial internal energies at lower temperatures.

The similar shapes (within experimental error) of the three breakdown diagrams in Fig. 5 indicate that the ion populations have similar distributions of internal energy while equilibrated at different temperatures. No significant broad-

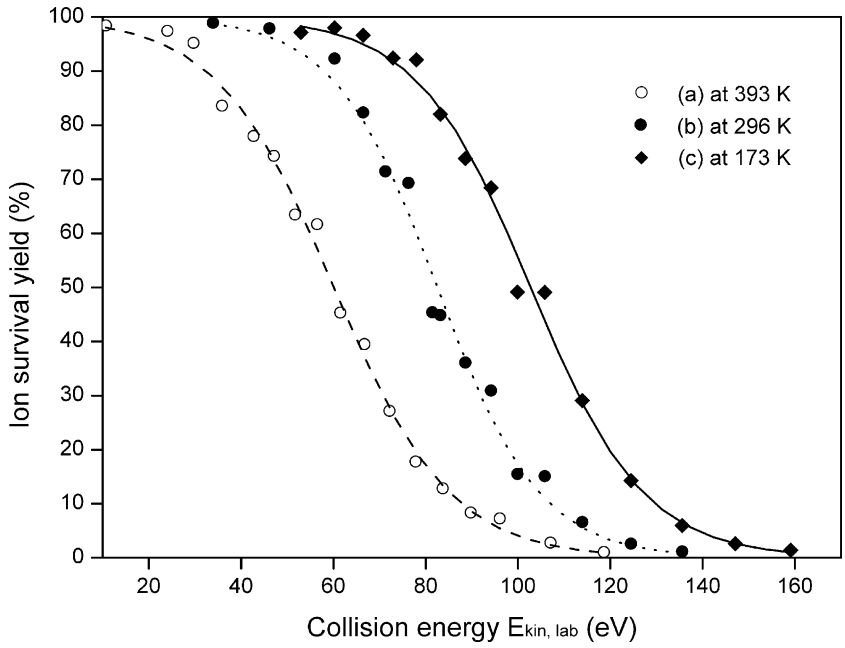

Fig. 5. A comparison of the typical on-resonance CAD breakdown diagrams of protonated leucine enkephalin obtained with the temperature-controlled cell at the temperatures of (a) 393 K, (b) 296 K, and (c) 173 K with the collision gas argon at the peak pressure of 5×10^{-6} mbar. The best-fit lines are Boltzmann sigmoidal curves in which the maxima and minima were set at 100 and 0%, respectively.

ening effects of the internal energy distribution were observed, which suggests that the temperatures of the ICR cell are homogenous and the thermalization of the ions with the new temperature-controlled cell efficiently influenced the temperature and internal energy of the ions.

The study demonstrates that the internal energy and the temperature of the trapped ion population can be changed in a well-controlled manner using the new ICR cell and that both high and low temperature studies are possible. This is imperative for both structure/conformation studies and fundamental energetic studies of large biomolecules in the gas phase, such as those reported in references [37–39] (which were performed using this cell).

5. Conclusions

The new FT-ICR ion cell described in this paper has been operated throughout the temperature range 77–438 K. Using direct heating and cooling, the temperature of the ICR cell has been changed in a controlled manner while ensuring a uniform temperature distribution. As a result, using a thermalization delay, the temperature of the ion population is well-defined and controlled. The experiments performed using the new cell indicated that the internal energy of the trapped ion population of the protonated model peptide changed with the cell temperature through a thermal equilibration. This allows a controlled manipulation of initial internal energy of the ion population through the entire temperature range 77–438 K, and makes it possible to perform experiments (such as ion dissociation, ion–molecule reactions, etc.) at temperatures much hotter and much cooler than room temperature. Finally, a novel protocol has been proposed to experimentally determine the geometry factor β of the new temperature-controlled cell by comparing the breakdown diagrams obtained with an ICR cell with a known geometry factor with those obtained using the new cell.

Acknowledgements

The authors gratefully acknowledge W. Barsinghorn and H. Alberda for their efforts in the successful construction of the new temperature-controlled ICR cell and Piet G. Kistemaker for carefully reading this manuscript. This work is part of the research program no. 49 “Mass spectrometric imaging and structural analysis of biomacromolecules” of the “Stichting voor Fundamenteel Onderzoek der Materie (FOM),” which is financially supported by the “Nederlandse organisatie voor Wetenschappelijk Onderzoek (NWO).” This research is also supported by FOM-project no. FOM-98PR1736. One of the authors (AAK) thanks the Swedish Foundation for International Cooperation in Research and Higher Education (STINT) for a research fellowship.

References

[1] A.G. Marshall, C.L. Hendrickson, G.S. Jackson, Mass Spectrom. Rev. 17 (1998) 1;
A.G. Marshall, Int. J. Mass Spectrom. 200 (2000) 331.
[2] B.S. Freiser, Acc. Chem. Res. 27 (1994) 353.

[3] R.P. Rodgers, K.V. Andersen, F.M. White, C.L. Henrickson, A.G. Marshall, Anal. Chem. 70 (1998) 4743.
[4] G.A. Valaskovic, N.K. Kelleher, F.W. McLafferty, Science 273 (1996) 1199.
[5] R.L. Hettich, M.V. Buchanan, Int. J. Mass Spectrom. Ion Proc. 111 (1991) 365;
J.A. Castoro, C. Koster, C. Wilkins, Rapid Commun. Mass Spectrom. 6 (1992) 239.
[6] M.L. Gross, D.L. Rempel, Science 226 (1984) 261;
M.B. Comisarow, A.G. Marshall, J. Mass Spectrom. 31 (1996) 581.
[7] M.V. Buchanan, R.L. Hettich, Anal. Chem. 65 (1993) 245A;
C.L. Holliman, D.L. Rempel, M.L. Gross, Mass Spectrom. Rev. 13 (1994) 105;
Y.T. Li, Y.L. Hsieh, J.D. Henion, M.W. Senko, F.W. McLafferty, B. Ganem, J. Am. Chem. Soc. 115 (1993) 8409;
R.D. Chen, X.H. Cheng, D.W. Mitchell, S.A. Hofstadler, Q.Y. Wu, A.L. Rockwood, M.G. Sherman, R.D. Smith, Anal. Chem. 67 (1995) 1159.
[8] F.W. McLafferty, Acc. Chem. Res. 27 (1994) 379.
[9] W.D. Price, P.D. Schnier, R.A. Jockusch, E.F. Strittmatter, E.R. Williams, J. Am. Chem. Soc. 118 (1996) 10640;
R.C. Dunbar, J. Phys. Chem. 98 (1994) 8705;
D. Tholmann, D.S. Thonner, T.B. McMahon, J. Phys. Chem. 98 (1994) 2002.
[10] F.W. McLafferty, Z.Q. Guan, U. Haupts, T.D. Wood, N.L. Kelleher, J. Am. Chem. Soc. 120 (1998) 4732.
[11] K.B. Breuker, H.B. Oh, D.M. Horn, B.A. Cerda, F.W. McLafferty, J. Am. Chem. Soc. 124 (2002) 6407.
[12] W.D. Price, P.D. Schnier, E.R. Williams, Anal. Chem. 68 (1996) 859;
R.A. Jochusch, P.D. Schnier, W.D. Price, E.F. Strittmatter, P.A. Demirev, E.R. Williams, Anal. Chem. 69 (1997) 1119;
D.S. Gross, Y. Zhao, E.R. Williams, J. Am. Soc. Mass Spectrom. 8 (1997) 519.
[13] P.D. Schnier, J.S. Klassen, E.F. Strittmatter, E.R. Williams, J. Am. Chem. Soc. 120 (1998) 9605;
J.S. Klassen, P.D. Schnier, E.R. Williams, J. Am. Soc. Mass Spectrom. 9 (1998) 1117;
E.R. Williams, R.A. Jochusch, J.C. Jurchen, S. Krishnaswamy, Proceedings of the 50th ASMS Conference on Mass Spectrometry and Allied Topics, Orlando, FL, June 2002;
E.N. Kitova, W. Wang, D.R. Bundle, J.S. Klassen, J. Am. Chem. Soc. 124 (2002) 13980.
[14] N. Felitsyn, E.N. Kitova, J.S. Klassen, Anal. Chem. 73 (2001) 4647.
[15] R.M.A. Heeren, K. Vekey, Rapid Commun. Mass Spectrom. 12 (1998) 1175;
R.M.A. Heeren, X. Guo, M.C. Duursma, L. Drahos, K. Vekey, Proceedings of the 49th ASMS Conference on Mass Spectrometry and Allied Topics, Chicago, IL, May 2001.
[16] E.W. Robinson, R.L. Wong, J.C. Jurchen, E.R. Williams, Proceedings of the 50th ASMS Conference on Mass Spectrometry and Allied Topics, Orlando, Fl, June 2002.
[17] H.-N. Lee, C.L. Hendrickson, A.G. Marshall, Proceedings of the 48th ASMS Conference on Mass Spectrometry and Allied Topics, Long Beach, CA, June 2000.
[18] H. Boehringer, F. Arnold, J. Chem. Phys. 77 (1982) 5534.
[19] N. Kobayashi, T. Kojima, Y. Kaneko, J. Phys. Soc. Jpn. 57 (1988) 1528;
H. Tanuma, M. Sakamoto, N. Kobayashi, Surf. Rev. Lett. 3 (1996) 205;
H. Tanuma, J. Sanderson, N. Kobayashi, J. Phys. Soc. Jpn. 68 (1999) 2570.
[20] J.A. Loo, Mass Spectrom. Rev. 16 (1997) 1;
C.V. Robinson, M. Gross, S.E. Radford, Method Enyzmol. 290 (1998) 296;
A. Miranker, C.V. Robinson, S.E. Radford, R.T. Aplin, C.M. Dobson, Science 262 (1993) 896.
[21] F. Wang, M.A. Freitas, A.G. Marshall, B.D. Sykes, Int. J. Mass Spectrom. 192 (1999) 319;
T.G. Venkateshwaran, J.T. Stewart, J.A.d. Haseth, M.G. Bartlett, J. Pharm. Biomed. Anal. 19 (1999) 709.
[22] S. Myung, E.R. Bradman, D.E. Clemmer, Proceedings of the 50th ASMS Conference on Mass Spectrometry and Allied Topics, Orlando, FL, June 2002;
E.R. Badman, C.S. Hoaglund-Hyzer, D.E. Clemmer, Anal. Chem. 73 (2001) 6000.
[23] S. Guan, Int. J. Mass Spectrom. 146/147 (1995) 261.
[24] M.B. Comisarow, Adv. Mass Spectrom. 8 (1980) 1698.
[25] D.L. Rempel, E.B. Ledford Jr., S.K. Huang, M.L. Gross, Anal. Chem. 59 (1987) 2527.
[26] S.H. Lee, K.-P. Wanczek, H. Hartmann, Adv. Mass Spectrom. 8 (1980) 1645.
[27] P. Caravatti, M. Allemann, Org. Mass Spectrom. 26 (1991) 514.
[28] S.C. Beu, D.A. Laude Jr., Int. J. Mass Spectrom. Ion Proc. 112 (1992) 215.
[29] G. Gabrielse, L. Haarsma, S.L. Rolston, Int. J. Mass Spectrom. Ion Proc. 88 (1989) 319.
[30] C.D. Hanson, M.E. Castron, E.L. Kerley, D.H. Russell, Anal. Chem. 61 (1989) 2528.
[31] S.K. Huang, D.L. Rempel, M.L. Gross, Int. J. Mass Spectrom. Ion Proc. 72 (1986) 15.
[32] V.H. Vartanian, D.A. Laude Jr., Int. J. Mass Spectrom. Ion Proc. 141 (1995) 189.
[33] M.E. Belov, R. Zhang, E.F. Strittmatter, D.C. Prior, K. Tang, R.D. Smith, Anal. Chem. 75 (2003) 4195.
[34] S.C. Beu, D.A. Laude Jr., Anal. Chem. 64 (1992) 177.
[35] National Instruments Corporation: Austin, USA.
[36] G.J. van Rooij, T. Mize, M. Konijnenburg, M. Seynen, A. Vijftigschild, R.M.A. Heeren, in preparation.
[37] X. Guo, M.C. Duursma, A. Al-Khalili, R.M.A. Heeren, Proceedings of the 50th ASMS Conference on Mass Spectrometry and Allied Topics, Orlando, FL, June 2002.
[38] X. Guo, M.C. Duursma, A. Al-Khalili, R.M.A. Heeren, Int. J. Mass Spectrom. 225 (2003) 71.
[39] X. Guo, M.C. Duursma, P.G. Kistemaker, R.M.A. Heeren, N.M.M. Nibbering, K. Vekey, J. Mass Spectrom. 38 (2003) 597.
[40] K. Vekey, J. Mass Spectrom. 31 (1996) 445.
[41] Y. Ge, D.M. Horn, F.W. McLafferty, Int. J. Mass Spectrom. 210/211 (2001) 203.
[42] P.B. O'Connor, Rapid Commun. Mass Spectrom. 16 (2002) 1160.
[43] P.B. Grosshans, A.G. Marshall, Int. J. Mass Spectrom. Ion Proc. 100 (1990) 347.
[44] H.L. Sievers, H.F. Grützmacher, P. Caravatti, Int. J. Mass Spectrom. Ion Proc. 157/158 (1996) 233.
[45] E.N. Nikolaev, M.V. Gorshkov, Int. J. Mass Spectrom. Ion Proc. 64 (1985) 115;
P. Kofel, M. Alleman, H.P. Kellerhals, K.P. Wanczek, Int. J. Mass Spectrom. Ion Proc. 74 (1986) 1;
P. Kofel, Ph.D., University of Bremen, 1987.
[46] R. Chen, A.G. Marshall, Int. J. Mass Spectrom. Ion Proc. 133 (1994) 29.
[47] D. Dahl, Idaho National and Environmental Laboratory, Idaho Falls, USA.
[48] L. Drahos, K. Vekey, J. Am. Soc. Mass Spectrom. 10 (1999) 323.